

# High-cycle fatigue life prediction of reinforced concrete deep beams



Benard Isojeh<sup>a,\*</sup>, Maria El-Zeghayar<sup>b</sup>, Frank J. Vecchio<sup>a</sup>

<sup>a</sup>University of Toronto, Civil Engineering Department, Canada

<sup>b</sup>Civil Engineer in the Renewable Power Business Unit at Hatch Ltd, Canada

## ARTICLE INFO

### Article history:

Received 14 October 2016

Revised 18 June 2017

Accepted 11 July 2017

Available online 20 July 2017

### Keywords:

Strut and tie

Fatigue

Fracture mechanics

Strain-life

High-cycle

Damage

## ABSTRACT

Concrete elements deteriorate as a result of continuous application of compressive fatigue loads. Irreversible deformation accumulates; hence, the effect on embedded steel reinforcing bars capacity and concrete resistance should be accounted for in the fatigue analysis of concrete structures. Experimental investigations were conducted to study the fatigue behaviour of eight small-scale reinforced concrete deep beams with a shear span to effective depth ratio of 1.25. Percentages of the diagonal cracking load from monotonic tests were used as fatigue loads. The deformation evolution within the shear spans of the deep beams were obtained by estimating the average principal and shear strain evolutions from the strain transformation analysis of LVDT (Linear Variable Displacement Transformer) data. Mid-span deflections and reinforcement strain evolutions with proximity to a major concrete crack location were obtained. In all beams, failure occurred with fracture of the longitudinal reinforcement at the intersection with the major concrete crack. Maximum strain evolutions for shear reinforcement measured at regions around the bends were observed to be lower than the strain evolutions observed in the longitudinal reinforcement. This was attributed to the governing arch mechanism common with deep beams.

The strut and tie method was modified to predict the fatigue life of the deep beams tested by modifying the constitutive models and effectiveness factor of concrete with fatigue damage models. To achieve this, the irreversible compressive fatigue strain in concrete is considered as a pseudo-load. The crack initiation life and the progressive crack growth of steel reinforcement are accounted for using strain-life models and linear elastic fracture mechanics, respectively. Within the developed algorithm, failure will occur when one of the evolving forces in either the concrete strut or steel reinforcement approaches the corresponding residual resistance capacity.

© 2017 Elsevier Ltd. All rights reserved.

## 1. Introduction

Investigations of the behaviour of reinforced concrete elements subjected to fatigue loading began in the twentieth century. Due to complex observations in the performances of the constituent materials, further interests in this field of study have evolved. From previous studies [1–3], failure of reinforced concrete elements due to the fracture of reinforcement at their intersection with concrete cracks, crushing of concrete, and excessive evolutions of diagonal tension cracks have been reported as modes of fatigue failure.

### 1.1. Mechanism of fatigue failure

The failure mechanisms observed in previous tests conducted on reinforced concrete beams were reported to be significantly

influenced by the shear span to effective depth ratio ( $a/d$ ), the stress ratio (ratio of the minimum stress to maximum stress), the reinforcement ratio, and the magnitude of fatigue load [4–6]. Fracture of the tensile reinforcement was observed to occur within the region of maximum moment within beams when subjected to smaller fatigue loads. On the other hand, shear failure due to diagonal cracking occurred under high fatigue loads [7]. The use of different reinforcement ratios have also been reported to influence the failure mechanisms [8]. For example, while lower reinforcement ratios are governed by the fracture of the reinforcement, heavily reinforced concrete members may fail due to crushing of concrete or diagonal tension cracks.

Reports on fatigue tests conducted on beams with shear reinforcement and having shear span to effective depth ratios greater than 2.0 showed increases in the shear reinforcement strains as diagonal or inclined cracks emanated [1–3]. The fatigue load transfer was described to involve a truss mechanism in which shear forces were transmitted by the shear reinforcement from one

\* Corresponding author at: M6J 1K1, 121 Wolesey st, Toronto, Ontario, Canada.  
E-mail address: [mb.isoje@mail.utoronto.ca](mailto:mb.isoje@mail.utoronto.ca) (B. Isojeh).

surface of an inclined compressive strut to an adjacent strut. Depending on the average induced strains or stresses in the reinforcement intersecting the diagonal cracks, localised crack growth in the shear reinforcement and widening of concrete cracks occurred. Fracture of the shear reinforcement typically occurred thereafter. However, beams with shear span to effective depth ratios lower than 2.0 were governed by arch mechanism and did not exhibit shear reinforcement fracture at failure [9].

Okamura et al. [1], Okamura and Ueda [2], and Ueda [3] reported that the increase in the shear reinforcement strain was proportional to the logarithm of the number of cycles leading to fracture, especially at bends. As the shear reinforcement fractured, collapse of the beams occurred where the remaining stirrup legs intersecting the widened inclined cracks were insufficient to withstand the applied maximum fatigue load. As such, the fatigue behaviour of shear reinforcement in terms of its maximum strain evolution up to yield was considered as a fatigue limit state. Models developed and reported by Okamura et al. [1], Hawkins [4], Higai [9], and Ruhnau [10] for estimating the strain within a shear span at any given cycle up to failure are used in the literature and codes of practice for this purpose.

Fatigue failure of deep beams with shear span to effective depth ratios of 1.0 and 1.5 were observed to fail under fatigue loading by crushing of concrete compressive struts, diagonal tension, or fracture of longitudinal reinforcement. No fracture of shear reinforcement was observed in any of the specimens [5,6]. In the tests conducted by Teng et al. [6], high-strength deformed steel bars and plain round steel bars were used as shear reinforcement in each shear span per beam. Results and crack patterns on both shear spans revealed no substantial difference. It was also observed that the shear reinforcement in the deep beams did not yield at failure.

An illustration of the behaviour of shear reinforcement in deep beams under fatigue loading can be observed from Higai's report [9] on moving load tests. According to Higai [9], as the distance between the moving load and the support reduced, the observed shear strength increased remarkably. Local compressive concrete stresses were also observed to develop in the vertical direction within the shear span; hence, decreasing the principal tensile stress in the concrete. In addition, it was reported that strains in stirrups decreased as the distance between the support region and loading point reduced. These observations are analogous to clamping or transverse compression stresses in deep beams under static loads [11,12]. However, further investigation is still required in order to understand the fatigue deformation of deep beams.

## 1.2. Design for fatigue resistance

Deep beam can be designed appropriately and conservatively under static loads using the strut and tie model. Basically, the required concrete section sizes and amount of reinforcement (dimensions of load transfer path) are obtained from the stresses estimated from the static loading conditions at failure (Ultimate Limit State) [13]. Under fatigue loading, the stresses induced in the load transfer paths are estimated from the proposed or given fatigue load (usually lower than the expected monotonic load at failure). The stresses in these paths are further normalised with the material strengths in order to obtain stress levels needed in fatigue models. As a means of fatigue damage resistance verification, the normalized stresses from fatigue loads are implemented into their corresponding fatigue stress-life models in order to obtain the number of cycles that will result in local deformation by crushing (in case of concrete) or fracture (in case of steel). For an appropriate design, the number of cycles leading to failure obtained is ensured to be more than the number of cycles expected for service life. To achieve this, the volumes of materials (section

size and amount of reinforcement) are generally increased, if need be [13].

The use of S-N models do not account for damage evolution of the structural element [14,15]. The norm in fatigue design of structures using stress-life models neglects the influence of irreversible strain accumulation in concrete which may be significant in fatigue life prediction. Further, knowledge of the deformation evolution within the shear spans of deep beams in terms of shear strains, principal tensile strains, and principal compressive strains under fatigue loading are expedient in understanding the behaviour of deep beams under fatigue loading, since their resistance capacities may be governed by the behaviour within the shear spans.

In this paper, the influence of load level, stress ratio, and longitudinal reinforcement ratio on the fatigue behaviour of deep beams with shear-span to effective depth ratio of 1.25 are investigated experimentally. An approach is developed using strut and tie analysis for predicting the fatigue life of deep beams. The evolution of irreversible strain accumulation, concrete strength and stiffness degradation, and reinforcement crack growth are accounted for in this approach.

## 2. Experimental program

### 2.1. Test specimens

In this investigation, beams with dimensions of  $175 \times 250 \times 700$  mm and an  $a/d$  value of 1.25 were used for fatigue tests (Fig. 1). The properties of the beams tested are given in Table 1 (columns 1–7). The reinforcement provisions used for the beams surpassed the minimum required in CSA A23.3-04 11.2.8.1 and 11.2.8.2 for shear, 10.5.1.2 for flexure [16], EC-1-1 (2004) 9.2.2 and 9.2.1.1 [17] for shear and flexure respectively, and ACI [18] Section R9.6.3.1 and R9.6.1.2 for shear and flexure respectively.

Adequate anchorage was provided based on code requirements in CSA- N12.13.1, N12.13.2 (shear reinforcement anchorage) [16], N12.5.2 (flexural reinforcement anchorage). The anchorage provisions also satisfied EC2-1-1 (2004) clause 8.5(1) and (2) for shear reinforcement and EC2-1-1 clause 8.4.1 (1) P for longitudinal reinforcement [17]. ACI Table 25-3-1 and Table 25.3.2 [18] for longitudinal and shear reinforcement, respectively were also used as provision benchmarks. Longitudinal reinforcement ratios of 0.45%, 0.90%, and 1.40% were provided, while 0.2% was used as the shear reinforcement ratio.

From Table 1, the first three beams (CONT-1 to -3) having longitudinal reinforcement ratios of 0.45%, 0.90%, and 1.40%, respectively, were tested monotonically, in order to obtain the load, corresponding to the diagonal cracking load. Once the cracking load was attained (based on readings from the LVDTs in tension), results from further increases in loading were not required. Percentages of the maximum diagonal cracking load were then used to define the fatigue loads for other beams with similar longitudinal reinforcement ratios.

The names attached to each beam tested under fatigue loading are indicative of the loading and reinforcement conditions; for example, C80-20-0 is assigned to a beam reinforced with 2-10 M (10 M refers to Canadian standard hot-rolled reinforcing bar with cross-section area of  $100 \text{ mm}^2$ ) and subjected to fatigue maximum and minimum loads of 80% and 20% of diagonal cracking load. The last value zero signifies 0.45% longitudinal reinforcement ratio. In the cases of beams C75-0-1 and C75-0-2, C75-0 signifies maximum and minimum fatigue loads of 75% and approximately 0%, respectively. The last numeral (1 or 2) represents 0.9% or 1.40% longitudinal reinforcement ratio, respectively.

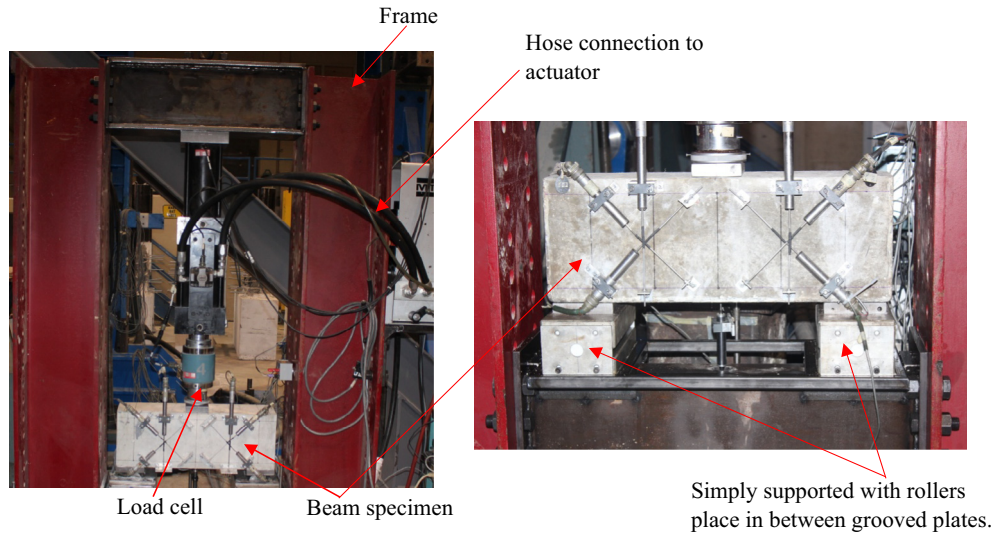


Fig. 1. Beam specimen setup.

**Table 1**  
Specimens description.

C1 Specimen name (#)	C2 $f_c$ (MPa)	C3 $\rho_l$ (%)	C4 (%)	C5 Max. load (% Pcr) kN	C6 Min. Load(kN)	C7 Cracking load Pcr (kN)	C8 Number of cycles to failure ( $N_f$ )
CONT-1	52.8	0.45	0.20	100	–	156.70	–
CONT-2	55.8	0.90	0.20	100	–	121.98	–
CONT-3	54.3	1.40	0.20	100	–	139.39	–
C80-0 (a)	46.6	0.45	0.20	80	5.0	–	460,000
C80-0 (b)	54.8	0.45	0.20	80	5.0	–	420,000
C75-0 (a)	57.1	0.45	0.20	75	5.0	–	770,000
C75-0 (b)	53.3	0.45	0.20	75	5.0	–	850,000
C70-0	52.2	0.45	0.20	70	5.0	–	1,500,000 <sup>a</sup>
C80-20-0	58.1	0.45	0.20	80	31.3	–	2,550,000 <sup>b</sup>
C75-0-1	52.4	0.90	0.20	75	5.0	–	3,000,000 <sup>a</sup>
C75-0-2	46.1	1.40	0.20	75	5.0	–	3,000,000 <sup>a</sup>

\*\*No failure (Stresses lower than endurance limit value or stress intensity factor lower than the threshold value).

<sup>a</sup> Test stopped without failure.

<sup>\*</sup> Number of cycles at first rebar fracture (final failure: 1,800,000).

<sup>b</sup> Number of cycles at first rebar fracture (final failure: 2,730,000).

## 2.2. Materials

A design compressive strength of 50 MPa (high strength concrete), having a mix ratio of 1:2:2 (cement: fine aggregate: coarse aggregate by weight) and a water/cement ratio of 0.5 was selected. This comprised of a maximum aggregate size of 10 mm and fine aggregate with a fineness modulus of 2.6. Slump readings between 80 and 150 mm were obtained during casting. At 28 days, the specimens were removed from the curing room and placed in a dry compartment afterwards. Canadian standard 15 M, 10 M (high-strength deformed steel reinforcing bars) and D4 (cold-worked) bars were used as reinforcement. The D4 reinforcing bars were used for the shear reinforcement, and the 2–10 M reinforcing bars for the hanger bars.

The average yield strength obtained based on coupon tests for the 15 M, 10 M, and D4 reinforcing bars were 430 MPa, 480 MPa, and 610 MPa respectively. The yield strength of the cold-worked steel rebar corresponded to the 0.2% offset strain.

## 2.3. Test setup

The setup for the fatigue tests consists of a servo-hydraulic testing equipment having a loading capacity of 350 kN. Each beam was

simply supported and the load was applied symmetrically through the load cell (Fig. 1). Strain gauges were attached to locations assumed to be cracking regions under fatigue loading. Hence, it was expected that under fatigue loading, provided diagonal inclined cracks occur, the strain evolution in the shear and longitudinal reinforcing bars may be observed. The surfaces of the reinforcement were initially filed lightly and cleaned with acid and base solutions. Subsequently, the strain gauges (5 mm size) were glued to the reinforcement surfaces. In order to prevent damage when in contact with concrete, the surfaces of the strain gauges were protected using aluminum foils. The wires connecting the strain gauges in the concrete were labelled appropriately and connected to data acquisition system channels. As the tests resumed, readings based on the connection to the channels were obtained progressively up to the point of failure.

The mid-span deflection per cycle was obtained using an attached LVDT positioned under the beam. The LVDTs attached to the concrete surfaces were used to obtain deformations in the respective directions. The observed deformations were subsequently used to estimate the average principal strains and shear strains per fatigue loading cycle. As indicated in the fifth and sixth columns of Table 1, percentages of the diagonal cracking loads observed from the monotonic tests were used as maximum and

minimum loads for the fatigue tests conducted, respectively. Each specimen was subjected to fatigue loading without a prior application of monotonic loading.

2.4. Test procedure

Initially, the three control beams CONT-1, -2, and -3 as indicated in Table 1 and Fig. 2, were tested under monotonic loading in order to obtain the diagonal cracking load (column 7). From Fig. 3, it can be observed that the capacities of CONT-2 and CONT-3 were approaching the limit of the testing machine; hence, each test was stopped having achieved the aim (obtaining the diagonal cracking load). Since the LVDTs attached to the surface of the beams could capture the cracking load, subsequent load values were not required. The diagonal cracking load for CONT-1 was observed to be higher than the values obtained for CONT-2 and CONT-3. This was attributed to the fact that heavily-reinforced deep beams are governed by shear deformations; hence, initial cracks under loading may be within the shear spans. On the other hand, lightly reinforced concrete deep beams are governed by

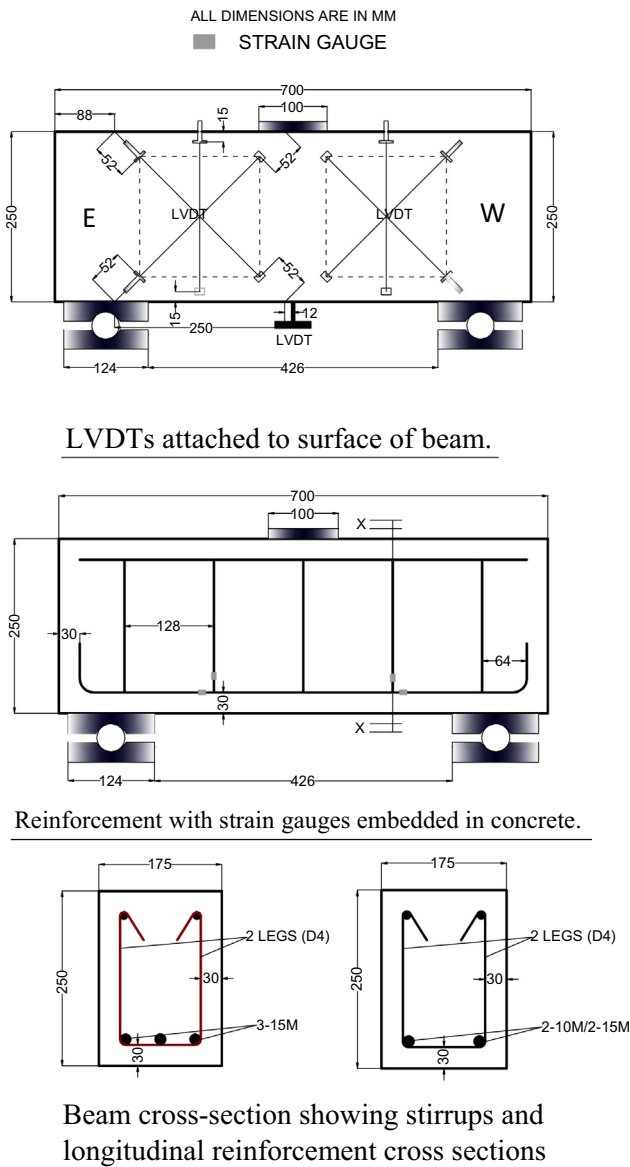
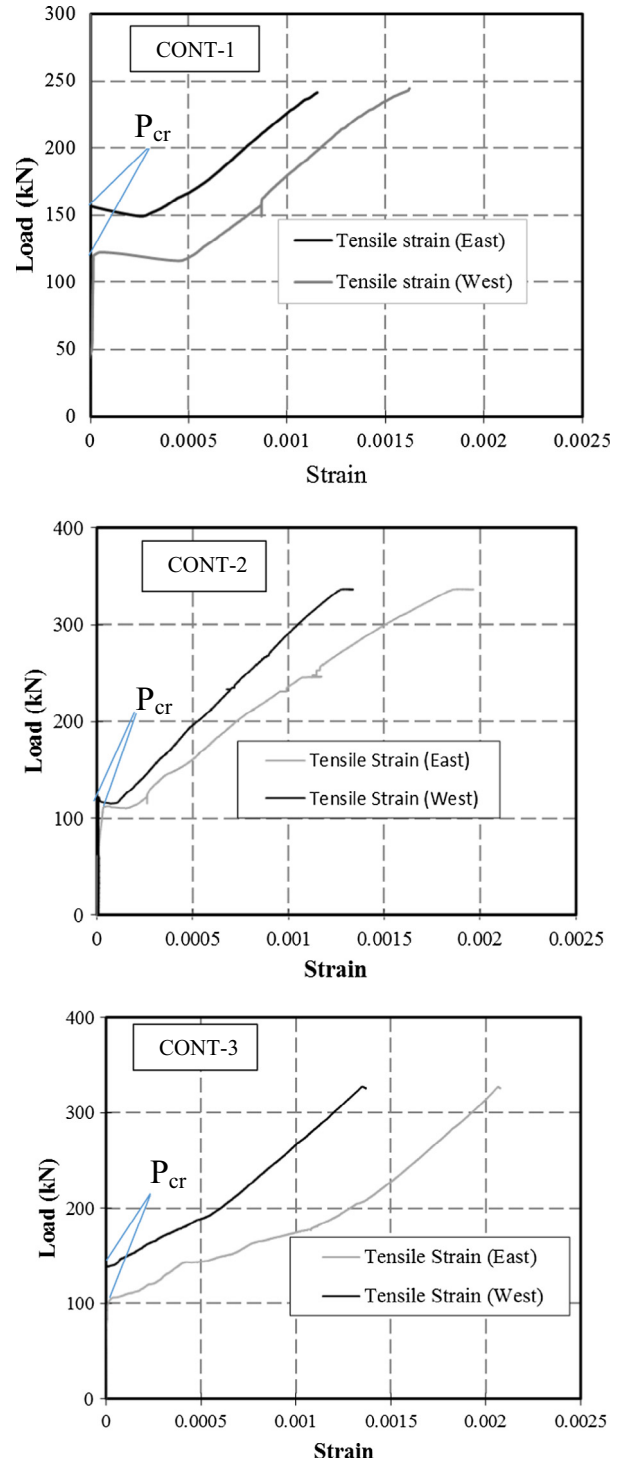


Fig. 2. Details of deep beam specimen.



flexural cracks within the mid-spans. Higher loads may be required for cracks to form within the shear spans of lightly reinforced beams.

For the fatigue loading, a pulsating load of a continuous sinusoidal waveform was generated from the loading equipment throughout the test duration. All fatigue tests were conducted at a frequency of 5 Hz and a minimum fatigue load of 5 kN was used, except for beam C80-20-0 where the minimum fatigue load was taken as 20% of the diagonal cracking load. The value was used to verify the influence of minimum fatigue loading on the fatigue life of the deep beams.

Although positive load ratios were considered in this investigation, structural components may be subjected to stress reversals (negative stress or load ratio) [19]. Based on investigations conducted by Zhang et al. [20], stress-life models obtained by plotting stress levels against the number of cycles to failure for different stress ratios, portrayed a reduction in the fatigue life of concrete as stress ratio reduced.

Further, the beams and the reinforcements used in this investigation are corrosion free. However, beams subjected to corrosion are significantly dependent on the frequency of loading [21].

### 2.5. Instrumentation

The LVDTs attached within the shear spans of each beam were used to measure the evolution of the average deformation (Figs. 1, 2, and 4). The average deformations in terms of the shear strains, the average principal strains, and the inclination of the principal tensile strain relative to the x- and y-directions within the shear spans of each beam were obtained from strain transformation of the LVDT data (Fig. 4).

$\varepsilon_1$  and  $\varepsilon_2$  are the average tensile and average compressive strain respectively. A program was developed to generate the deformation evolutions from the laboratory data.

For the West LVDTs, (where  $\gamma_{xy}$  is positive, and  $\varepsilon_y = e_b$ )

$$\varepsilon_x = e_c - e_b + e_a$$

$$\gamma_{xy} = e_a - e_c \quad (1)$$

For the East LVDTs, ( $\gamma_{xy}$  is negative, and  $\varepsilon_y = e_b$ )

$$\varepsilon_x = e_c - e_b + e_a$$

$$\gamma_{xy} = e_c - e_a \quad (2)$$

The average principal concrete strains using Mohr circle of strains were obtained thus:

$$\varepsilon_{1,2} = \frac{1}{2}(\varepsilon_x + \varepsilon_y) \pm \frac{1}{2} \left( \sqrt{(\varepsilon_x - \varepsilon_y)^2 + \gamma_{xy}^2} \right) \quad (3)$$

The values for the evolution of  $\theta$ , the inclination of the principal tensile strain direction relative to horizontal, was estimated using  $\gamma_{xy}$  (shear strain),  $\varepsilon_x$  (average strain in the horizontal direction), and  $\varepsilon_y$  (average strain in the vertical direction).

In order to obtain the load corresponding to the diagonal cracking load, readings were obtained from LVDTs measuring tensile strains ( $e_a$ ) as shown in Fig. 4. From each reading, the load corresponding to the diagonal cracking was taken as the load at

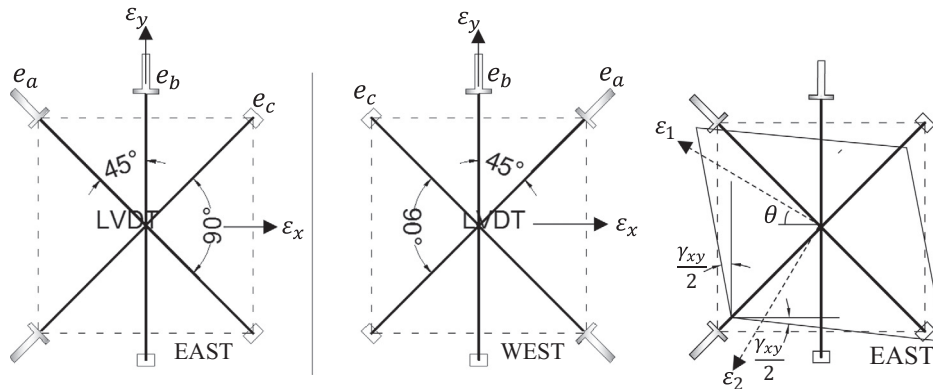


Fig. 4. LVDTs strain transformation.

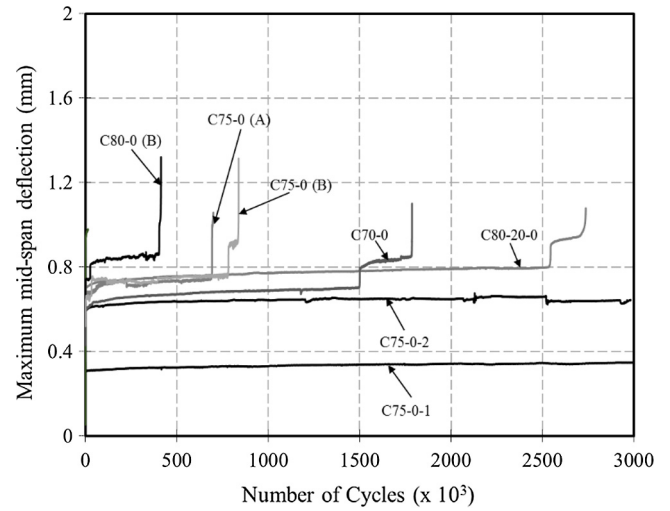


Fig. 5. Evolution of mid-span deflection.

which the slope of the deformation curve began to change significantly.

The results of the experiments conducted are presented subsequently. Figs. 5–9 show mid-span deflections, the crack patterns, principal strain evolutions (tensile and compressive) and shear strain evolutions.

### 3. Test results

The number of cycles leading to failure are given in Table 2. Specimens C75-0-1 and C75-0-2 were stopped at 3,000,000 cycles since no signs of failure were apparent. Although beam C75-0 failed at about 800,000 cycles, the fatigue load used was slightly higher compared to C75-0-1 and C75-0-2. It is well-known that fatigue life increases as the reinforcement ratio increases under a given load. However, the high fatigue load used for beam C75-0 may have resulted in the large difference between observed fatigue cycles when compared with beams C75-0-1 and C75-0-2.

#### 3.1. Mid-span deflection/ stiffness degradation

The mid-span deflections of seven specimens are given in Fig. 5. The applied fatigue load influenced the evolution of the mid-span deflection of the beams having the same reinforcement ratios (C70-0, C75-0 (A), C75-0 (B), and C80-0 (B)) (2–10 M rebars). As

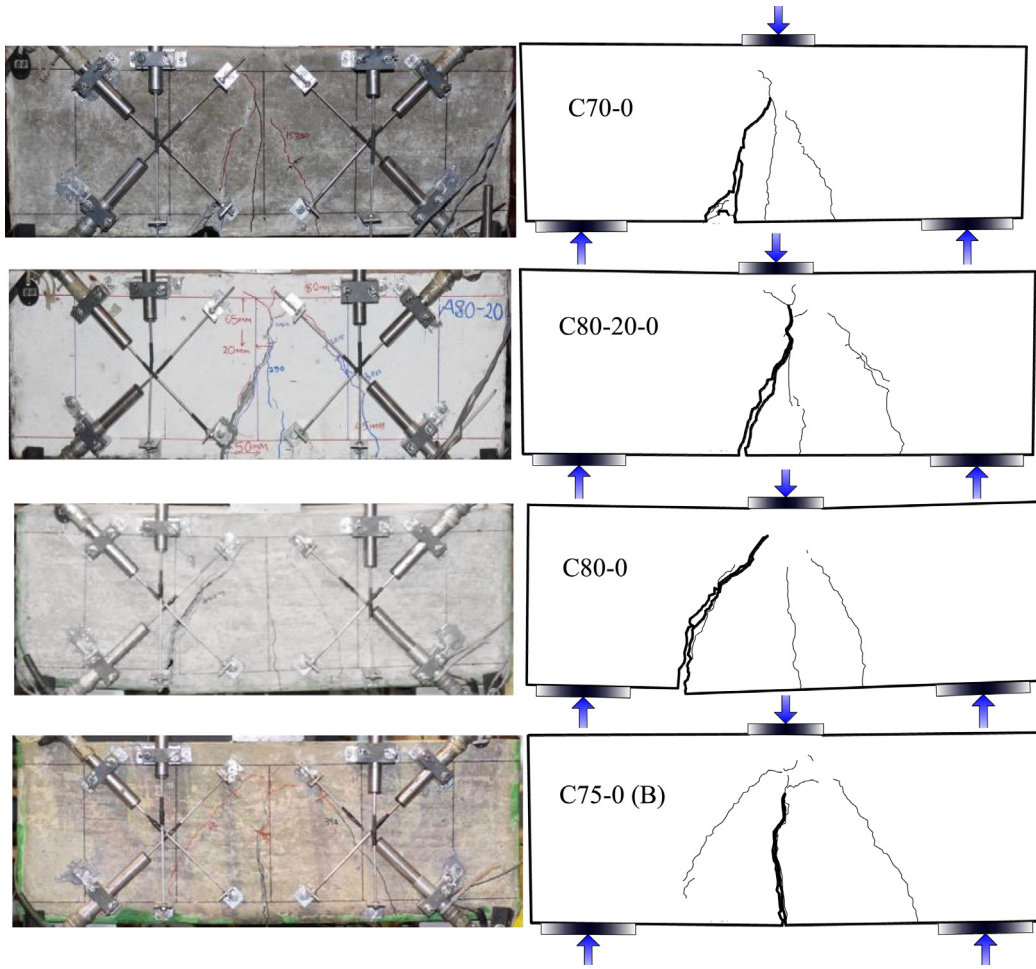


Fig. 6. Crack pattern and shear-span fatigue degradation.

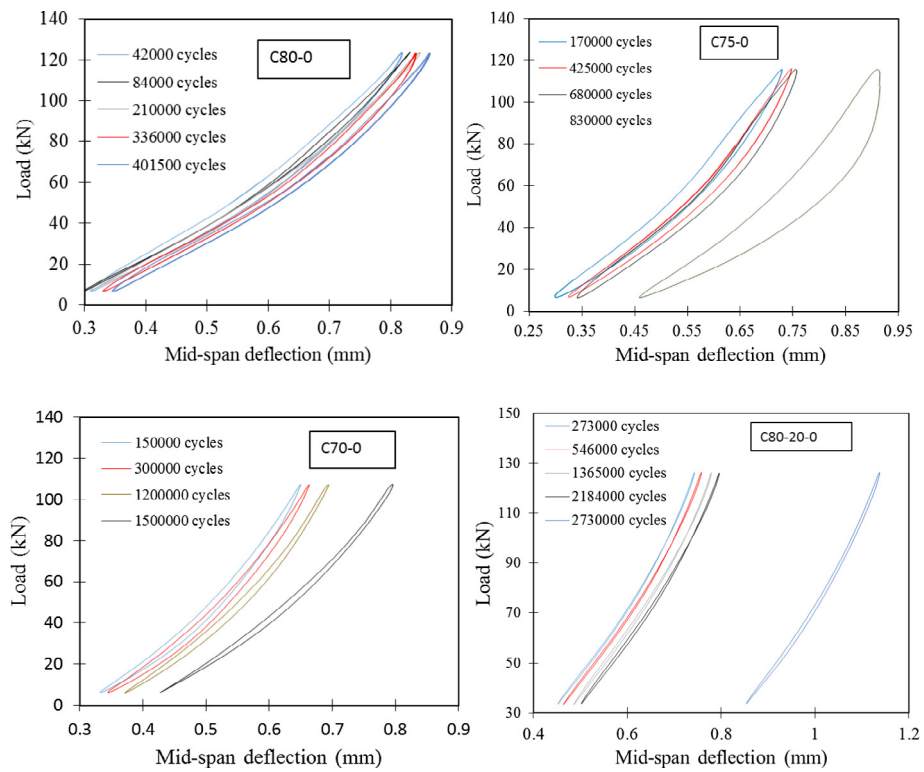


Fig. 7. Fatigue hysteresis loops.

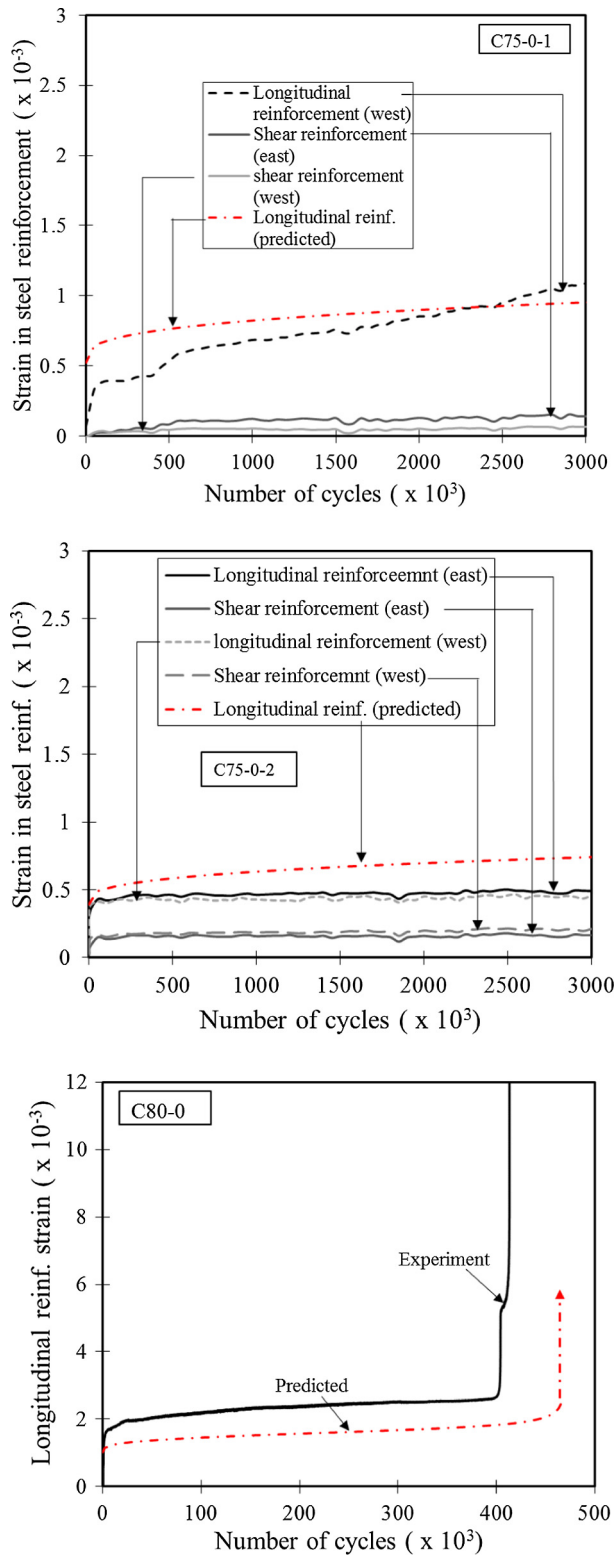


Fig. 8. Strain evolution in reinforcing bars.

the stress level increased, the deflection and the evolving rate increased. The specimens failed finally at 1,800,000, 770,000, 850,000, and 420,000 cycles, respectively.

For similar maximum load levels (C80-0 and C80-20), an increase in the minimum load level (20% of diagonal cracking load) resulted in the reduction of the mid-span deflection and its rate of

evolution, and an increase in fatigue life. The failure of specimen C80-20 occurred after 2,730,000 cycles. By comparing beams reinforced with 10 M and 15 M rebars, it can be deduced that beams with higher longitudinal reinforcement ratios exhibited lower deflection. Although beam C75-0-2 with 3–15 M rebars exhibited a higher initial deflection (due to stochastic behaviour of concrete) compared to C75-0-1, the rate of increase of deflection with fatigue cycles was observed to be lower in C75-0-2 (see Fig. 5) because beam C75-0-2 was reinforced with 3–15 M reinforcing bars, whereas, C75-0-1 was reinforced with 2–15 M reinforcing bars. Hence, lower stresses and strains per cycle were induced in the former. The influence of reinforcement ratio can also be observed in the strain evolution plot for longitudinal reinforcing bars (considered in a subsequent section).

The crack patterns of beams C70-0, C80-20-0, C80-0, and C75-0 (b) are shown in Fig. 6. Inclined or shear-flexural cracks formed within the shear-spans of C80-0 and C80-20-0 at the initial stage of fatigue loading. For beam C80-0, a flexural crack at the mid-span region was initially observed; however, the propagation of the inclined crack due to a high fatigue load range prevailed, while no progressive opening of the flexural crack at the mid-span occurred. In other beams (C75-0, C70-0), flexural cracks occurred at the initial stage of fatigue loading. The applied fatigue load range was insufficient (low) to result in a shear-flexural crack at the initial stage. Although the development of inclined cracks away from the mid-span regions occurred afterwards due to the degradation of the tensile strength of concrete to a value corresponding to the induced tensile stress within the plane, the reinforcement fatigue damage within the mid-span region had increased substantially before the emergence of the inclined cracks and initiation of rebar damage growth (crack propagation); hence, the observed failure occurred within the mid-span region. In beam C80-20-0, the maximum fatigue load resulted in a diagonal crack in beam C80-20-0 at the initial stage of fatigue loading cycles; however, the damage concentration within the mid-span region was also attributed to the increased minimum fatigue load which resulted in a low fatigue load range. This behaviour supports the observation by Chang and Kesler [7] regarding the influence of fatigue load on failure regions.

The degradation of the beams under fatigue loading can also be observed from the hysteresis loops obtained from each tested specimen (Fig. 7). As the minimum fatigue load increased, the degradation or inclination of each hysteresis loop towards the abscissa tends to decrease (C80-0 and C80-20-0). As the fatigue load range increased, a corresponding increase in the degradation of the hysteresis loops was also observed. The large increase in mid-span deflection between hysteresis loops as indicated in C75-0, C70-0, and C80-20-0 indicates reinforcement fracture or substantial crack.

### 3.2. Shear-span deformation

Within the shear-span, the average shear strain, the average principal compressive strain evolution and the average tensile strain evolution were monitored. In addition, the strain evolution on the reinforcing bars (shear and longitudinal) at regions within the shear-spans were observed. As shown in Fig. 8, the strain evolutions in the longitudinal reinforcing bars in beams C75-0-1 and C75-0-2 were higher than the strain evolutions in the shear reinforcement. This further supports the prominence of the arch mechanism (load transfer path) behaviour and the obvious reason for fracture of longitudinal reinforcing bars instead of shear reinforcement. In addition, as a result of lower reinforcement ratio in beam C75-0-1, higher strain evolution data were observed when compared to specimen C75-0-2.

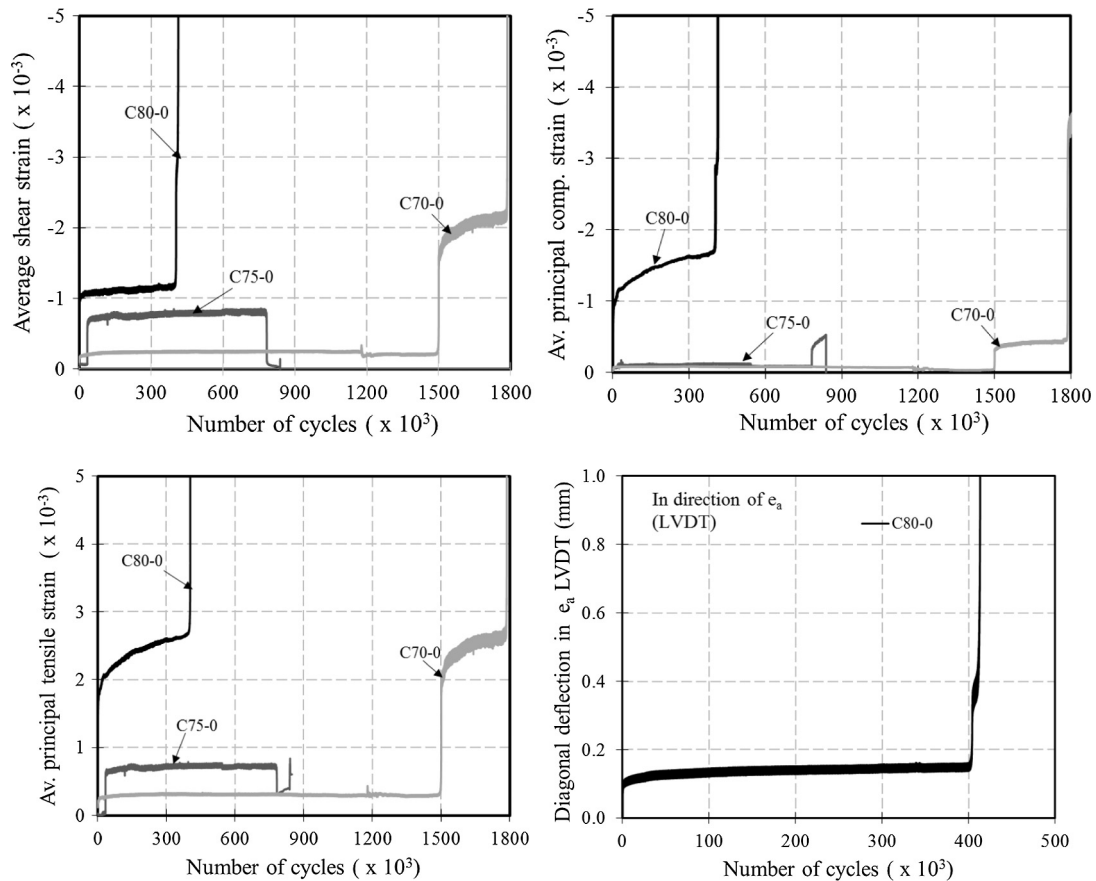


Fig. 9. Average principal and shear strain evolutions, and diagonal deformation (C80-0).

Table 2  
Fatigue test results and predictions.

C1 Specimen name (#)	C2 Number of cycles to failure $N_f$ (Log $N_f$ )	C3 Predicted number of cycles to failure $N_f$ (Log $N_f$ )	C4 Helgason et al. [24]/ AASHTO [25] predictions (Log $N_f$ )
C80-0 (a)	460,000 (5.7)	466,000 (5.7)	350,000 (5.5)
C80-0 (b)	420,000 (5.6)	466,000 (5.7)	350,000 (5.5)
C75-0 (a)	770,000 (5.9)	842,000 (5.9)	450,000 (5.7)
C75-0 (b)	850,000 (5.9)	842,000 (5.9)	450,000 (5.7)
C70-0	1,500,000 <sup>c</sup> (6.2)	1,060,000 (6.0)	530,000 (5.7)
C80-20-0	2,550,000 <sup>b</sup> (6.4)	1,640,000 (6.2)	**
C75-0-1	3,000,000 <sup>a</sup>	**	**
C75-0-2	3,000,000 <sup>a</sup>	**	**

<sup>a</sup> Test stopped without failure.

<sup>\*</sup> Number of cycles at first rebar fracture (final failure: 1,800,000).

<sup>b</sup> Number of cycles at first rebar fracture (final failure: 2,730,000).

\*\* No failure (Stresses lower than endurance limit value or stress intensity factor lower than the threshold value).

The analysis involved in the prediction of the strain evolutions will be discussed in a subsequent section (including beam C80-0).

In Fig. 9, it can be observed that for beams (C80-0, C75-0, and C70-0) with similar reinforcement ratios, the shear-span deformations in terms of average shear strain, average principal compressive and tensile strain evolutions (estimated using strain transformation equations) increased as the fatigue load level increased. Since the fatigue behaviour of beams C75-0 and C70-0 was governed by the reinforcement crack growth at the mid-span after concrete cracking, the mechanism which involved the transfer of forces through the compressive strut to the support was altered due to localised behaviour at the mid-span as the

reinforcement crack propagated. As such, the compressive strain within the shear span and its corresponding evolution, alongside the average shear and average principal tensile strains for beams C75-0 and C70-0 were almost constant except towards failure (see Fig. 9). In addition, the diagonal deformation (within the shear-span where failure occurred) in the direction of the LVDT in tension for specimen C80-0, was observed to evolve as the fatigue loading cycles increased.

#### 4. Fatigue life verification using strut and tie model

Under monotonic loading, an insight to the flow of forces in a deep beam can be obtained using strut and tie models. The internal flow of forces is represented using concrete compressive struts and reinforcement ties, while they meet at nodes. Since this concept is based on the lower bound theorem, equilibrium conditions must be fulfilled and yield condition is not violated. A mechanism occurs once plasticity develops. Stresses in concrete are limited to the crushing strength, while steel reinforcement is governed by the yield value [22,23].

Under fatigue loading, the initial stresses in steel and concrete are lower than the limiting capacity along the stress trajectory (see Fig. 10). As the number of cycles increase, the induced stress in concrete increases, irreversible strain accumulates, and the limit strength decreases. Further, an increase in steel stress due to crack growth occurs. Provided models can be developed to account for the instant of a mechanism due to the progressive deterioration, then the fatigue life of the structure can be predicted.

From the experimental results reported herein, the collapse due to fatigue failure of each beam was governed by the fracture of

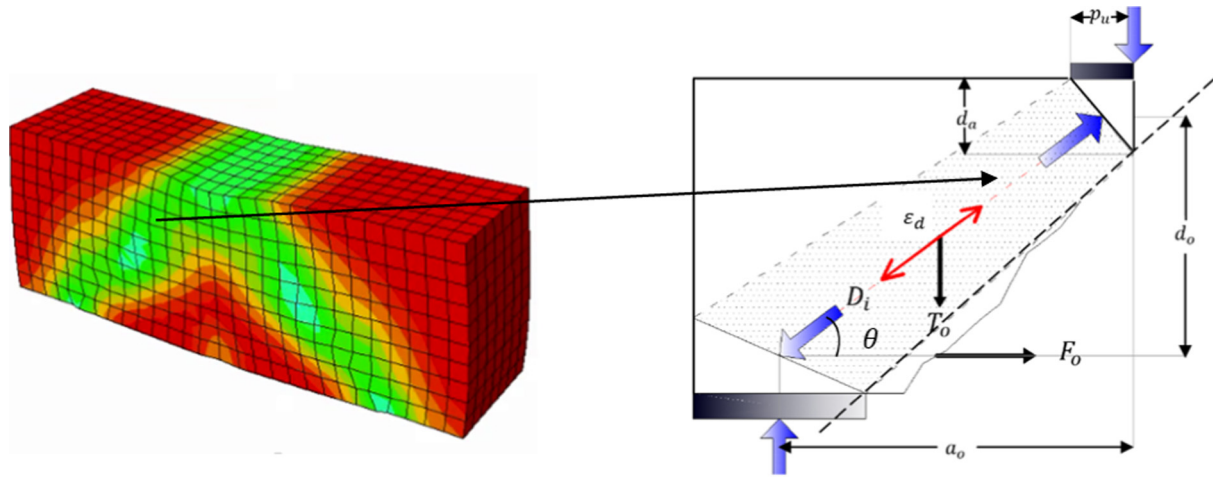


Fig. 10. Strut and tie model for a deep beam under fatigue loading.

longitudinal reinforcing bars under fatigue loading. It was postulated previously that this behaviour is attributed to the fact that load is transferred to the support from the loading point through arch mechanism and not by truss action common with beams having shear-span to effective depth ratios greater than 2.0.

In the analysis of fatigue loading, the deterioration of material properties such as concrete strength, steel residual area after crack growth, and the irreversible compressive strain accumulation can be accounted for in the constitutive, compatibility, and equilibrium equations of an analysis algorithm such as strut and tie. As such, a reinforced concrete beam damaged due to fatigue may fail when reloaded statically up to the same fatigue load after a given number of cycles. At the point of failure, crushing of concrete struts or fracture of reinforcing bars (shear or longitudinal, depending on the  $a/d$  value) may govern when the acting force in either the concrete or steel reinforcing bars becomes equal to the corresponding resistance capacity. The number of cycles at which this occurs is termed the fatigue life of the structural element.

To further illustrate this concept, the numbers of cycles leading to failure for each beam tested in this investigation were predicted. The predicted numbers of cycles were compared with those obtained using Helgason et al. [24] (used by AASHTO [25]). The fatigue load used for prediction was taken as the average load from the two curves for the CONT-1, CONT-2 and CONT-3 beams (Fig. 2).

#### 4.1. Fatigue equilibrium equation

From Fig. 10,

$$F_o = A(i)E_s\epsilon_x \quad (4)$$

$$T_o = A_vE_s\epsilon_v \quad (5)$$

$$D_i = f_{c2}w(p_u\sin\theta + d_a\cos\theta) \quad (6)$$

Under fatigue loading, the irreversible strain ( $\epsilon_d$ ) is considered as a pseudo-load. The value is assumed to be zero at the first cycle [26]. For subsequent cycles,

$$F_{ed} = E_{cfat}\epsilon_d w(p_u\sin\theta + d_a\cos\theta) \quad (7)$$

In Fig. 10 and Eqs. (4)–(7),  $F_o$  is the force in the longitudinal reinforcement,  $A(i)$  is the residual longitudinal reinforcement area (function of reinforcement crack growth),  $E_s$  is the elastic modulus of steel reinforcement,  $\epsilon_x$  is the strain in the longitudinal reinforcement,  $T_o$  is the force in the shear reinforcement within the shear span,  $A_v$  is the area of shear reinforcement within the shear span,

$\epsilon_v$  is the assumed strain in the shear reinforcement,  $D_i$  is the compressive force in the concrete strut,  $f_{c2}$  is the compressive stress in the concrete strut (function of concrete damage evolution),  $w$  is the width of the beam,  $p_u$  is taken as half of the loading plate length,  $\theta$  is the inclination of the compressive strut to the horizontal,  $d_a$  is the depth of the nodal zone under the loading plate,  $F_{ed}$  is the pseudo-load due to irreversible strain accumulation,  $E_{cfat}$  is the residual stiffness of concrete strut, and  $\epsilon_d$  is the irreversible fatigue strain.

#### 4.2. Fatigue constitutive models

The fatigue constitutive models used for concrete under compression fatigue loading and the corresponding irreversible strain ( $\epsilon_d$ ) model have been previously developed by the authors [27,28]. These models were used in this investigation for the fatigue damage analysis of concrete. Eqs. (8) and (9) are constitutive models for normal strength concrete using Hognestad's equation. Using Hognestad's Equation [29] for concrete compressive stress–strain model, the stress in a fatigue-damaged strut is expressed as [28]:

$$\left(\frac{\epsilon_{c2}}{\epsilon_c^*}\right)^2 - \frac{2\epsilon_{c2}}{\epsilon_c^*} + \frac{f_{c2}}{f_p(1-D_{fc})} = 0 \quad (8)$$

$$\epsilon_c^* = \epsilon_p \left(1 + \sqrt{D_{fc}}\right) - \epsilon_d \quad (9)$$

$f_{c2}$  is the principal compressive stress,  $f_p$  is the peak concrete compressive stress (equal to  $f'_c$ ),  $\epsilon_p$  is the compressive strain corresponding to  $f_p$ ,  $\epsilon_{c2}$  is the average net strain in the principal compressive direction, and  $\epsilon_c^*$  is the strain corresponding to the peak stress of the degraded concrete strength. Models for  $D_{fc}$  and  $\epsilon_d$  can be obtained from [27,28], respectively.

The total fatigue life of steel reinforcement can be assumed to constitute the crack initiation life (controlled by localised plasticity-crack nucleation) and the crack propagation life. For ductile materials, the crack initiation life is usually lower than the crack propagation life. However, the reverse is true for brittle materials. The strain-life approach which considers localised plasticity was used to obtain the crack initiation life, while fracture mechanics was used to estimate the crack propagation life from an initial crack length [30]. The localised stress and strain on the reinforcement at the intersection with concrete crack can be obtained using finite element analysis modelling or simply by Neuber's rule (Eq. (10)). The Neuber's rule is often used to extrapolate

elastic analysis so that stresses and strains associated with the effects of local yielding can be obtained.

$$\sigma\varepsilon = \frac{(K_t S)^2}{E} \quad (10)$$

$K_t$  is the stress concentration factor, and  $S$  is the nominal stress.  $\sigma$  and  $\varepsilon$  are the localised stress and strain, respectively. The mean value of  $K_t$  (depending on the reinforcement geometries) was obtained as 1.9 from a table and chart provided by Jhamb and MacGregor's [31] on stress concentration factors for reinforcing bars. In order to express the material properties of steel in the form of a cyclic stress-strain and strain-life curve, Masing's model and Smith-Watson-Topper (SWT) approach expressed in Eqs. (11) and (12) respectively, were used [32,33]. The SWT model is empirically based and accounts for the effect of mean stresses on fatigue behaviour. The SWT model relates the product of the maximum stress and total strain amplitude ( $\sigma_{max}\varepsilon_a$ ) to the fatigue life. The total strain consist of the summation of elastic and plastic terms. From the model, the product of the stress amplitude and strain amplitude for a fully reversed test is equal to  $\sigma_{max}\varepsilon_a$  for a mean stress test [34]. The parameters (mean test values) in the model  $\sigma'_f$ ,  $b$ ,  $c$ ,  $\varepsilon'_f$  are fitting constants which are essentially material properties.

$$\varepsilon_a = \frac{\sigma_a}{E} + \left(\frac{\sigma_a}{H'}\right)^{1/n'} \quad (11)$$

$$\sigma_{max}\varepsilon_a = \frac{(\sigma'_f)^2}{E} (2N_f)^{2b} + \sigma'_f\varepsilon'_f(2N_f)^{b+c} \quad (12)$$

The approach for estimating  $\sigma_{max}$ ,  $\varepsilon_{max}$  (maximum stress and strain at notch),  $\sigma_a$ ,  $\varepsilon_a$  (stress amplitude and corresponding strain) are illustrated in [33,35]. From Boller and Seeger [35], parameters in Eqs. (11) and (12) common to the tests conducted in this investigation (mean test values) are given as:

$$b = -0.087, \quad c = -0.58, \quad \varepsilon'_f = 0.59, \quad \sigma'_f = 720 \text{ MPa},$$

$$n' = b/c = 0.15, \quad H' = \frac{\sigma'_f}{\varepsilon_f^{n'}} = 779.3 \text{ MPa}.$$

For the crack propagation life prediction, the residual area of the cracked reinforcement was estimated using the approach and formulas reported in [26], reproduced in Fig. 11 and Eqs. (13) and (14):

$$A(a_y) = \frac{\theta}{90} \pi r^2 - r \sin\theta(2r - a_y) \quad (13)$$

$$\theta = \cos^{-1}\left(\frac{r - 0.5a_y}{r}\right) \quad (14)$$

$A(a_y)$  is the area of the fractured surface of a steel reinforcing bar,  $\theta$  is shown in Fig. 11,  $a_y$  is the crack depth, and  $r$  is the radius of the

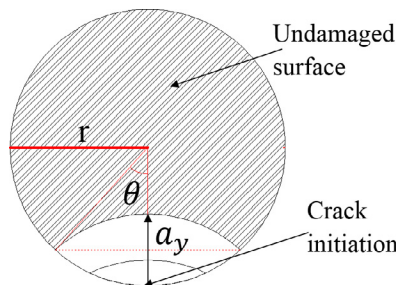


Fig. 11. Crack growth on a reinforcing bar surface.

reinforcing bar. The fracture mechanics models for estimating  $a_y$ , the initial crack, and the shape factor have been reported in [26].

### 4.3. Reinforcement crack growth

From the Paris crack growth law (Eq. (15)), the propagation of a reinforcing bar crack can be predicted, as a function of stress intensity factor range ( $\Delta K$ ) (Eq. (16)). The parameter  $\Delta K$  is generally expressed as a function of the fatigue stress range ( $\Delta\sigma$ ), crack size ( $a$ ) and a shape factor ( $Y$ ) for the reinforcing bar [34,36–38].

$$\frac{da}{dN} = C\Delta K^n \quad (15)$$

$$\Delta K = Y \cdot \Delta\sigma \cdot \sqrt{\pi a} \quad (16)$$

The crack depth ( $a_j$ ) for a given number of cycles is estimated from Eqs. (15) and (16) thus:

$$a_j = \left( \frac{a_i^\alpha}{1 - [N_{ij}(C \cdot \alpha \cdot \pi^{\frac{n}{2}} \cdot Y^n \cdot \Delta\sigma^n \cdot a_i^\alpha)]} \right)^{\frac{1}{\alpha}} \quad (17)$$

where  $\alpha = (n/2) - 1$ .

$a_i$  and  $a_j$  are the smallest and largest crack depth for the interval of cycles considered ( $N_{ij}$ ). However, the estimation of  $a_j$  requires the value of  $a_i$ , which is the previous crack depth [35].  $Y$  is the shape factor. The initial minimum crack can be obtained iteratively from (Eq. (18)) [38]:

$$a_o = \frac{1}{\pi} \left( \frac{\Delta K_{th}}{Y \Delta\sigma_{lim}} \right)^2 \quad (18)$$

where  $\Delta\sigma_{lim}$  corresponds to the fatigue limit stress at which fatigue damage will not initiate, and  $\Delta K_{th}$  is the threshold stress intensity factor. The crack does not propagate for stress intensity values lower than  $\Delta K_{th}$ . However, the threshold intensity factor was taken as 5 MPa  $\sqrt{\text{m}}$  [39] (m is in metres). An equation for the shape factor, recommended in BS 7910 (1999) as a function of the crack depth, is given in Eq. (19) [40].

$$Y = \frac{1.84}{\pi} \left\{ \tan\left(\frac{\pi a}{4r}\right) / \left(\frac{\pi a}{4r}\right) \right\}^{0.5} \cos\left(\frac{\pi a}{4r}\right) \left[ 0.75 + 2.02\left(\frac{a}{2r}\right) + 0.37\left\{1 - \sin\left(\frac{\pi a}{4r}\right)\right\}^3 \right] \quad (19)$$

where  $r$  is the radius of the reinforcing bar and  $a$  is the crack depth.

The residual area of reinforcement  $A(i)$  required in Eq. (4) was obtained by subtracting the area of the fractured surface from the initial reinforcing bar area. It was assumed that the stresses induced in the reinforcing bars on the same layer in a beam cross-section are equal. As such, the progressive reduced area can be obtained by multiplying the initial area of reinforcement or reinforcement ratio by the ratio of a residual rebar area to its uncracked area.

### 4.4. Compatibility equation

From Mohr's circle of strain, the relationship between the strain in the horizontal direction, the principal tensile strain and the principal compressive strain can be estimated from:

$$\varepsilon_{c1} = \varepsilon_x + (\varepsilon_x - \varepsilon_{c2})\cot^2\theta \quad (20)$$

where  $\varepsilon_{c1}$  is the average effective principal tensile strain,  $\varepsilon_x$  is the average strain in the horizontal direction,  $\varepsilon_{c2}$  is the average effective principal compressive strain, and  $\theta$  is the inclination of the compressive strut. The average strain in the vertical direction (required in Eq. (5)) within the shear span was estimated as:

$$\varepsilon_v = 0.5\varepsilon_{c1}(1 - \cos 2\theta) + 0.5\varepsilon_{c2}(1 + \cos 2\theta) \quad (21)$$

Since appropriate anchorage was ensured based on design specification, perfect bond was assumed in this investigation. Hence, the horizontal strain  $\varepsilon_x$  is taken as the strain in the longitudinal reinforcement, while the vertical strain  $\varepsilon_v$  is the strain in the shear reinforcement within the shear-span. In this approach, it was also assumed that cracks do not propagate on the shear reinforcement

as the number of cycles increase. This is attributed to the fact that the estimated forces in shear reinforcement are overly conservative since the contributions of other mechanisms such as aggregate interlock and clamping effects were neglected. This approach was used to estimate the number of cycles at which the fracture of the longitudinal reinforcing bars at the intersection with a concrete crack will occur. The algorithm used is shown in Fig. 12. Basically,

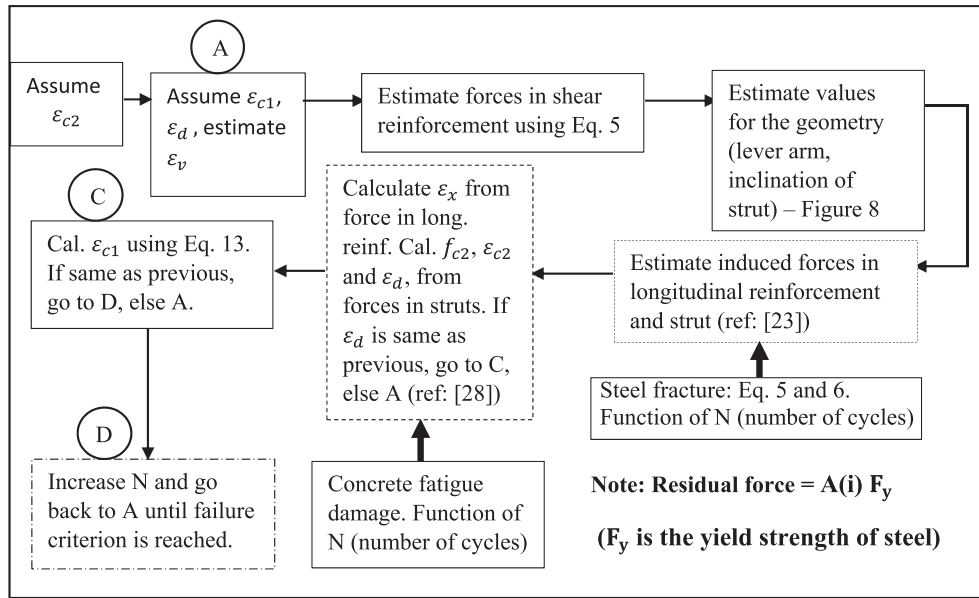


Fig. 12. Algorithm for predicting the fatigue life of a deep beam.

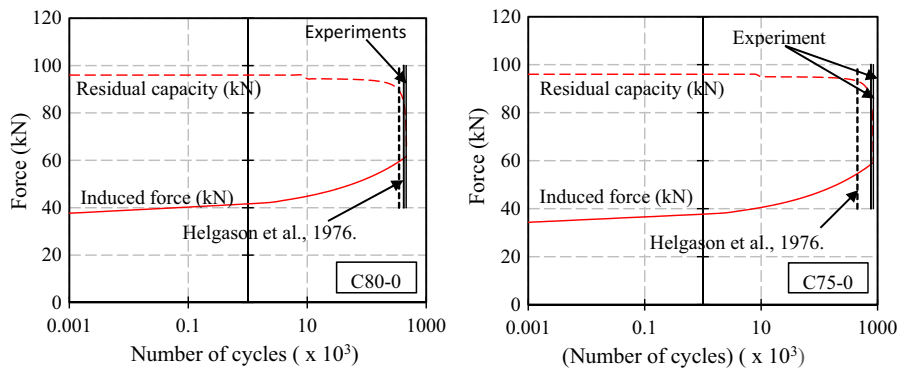


Fig. 13. Fatigue life prediction from strut and tie (C80-0 and C75-0).

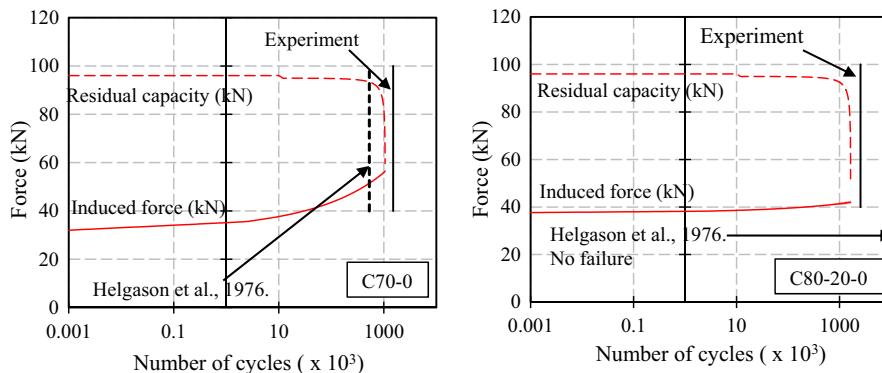


Fig. 14. Fatigue life prediction from strut and tie (C70-0 and C80-20).

the equilibrium, compatibility, and constitutive equations are satisfied for each cycle of fatigue loading considered while accounting for the progressive damage and area reduction of the strut and tie, respectively, until the governing failure criterion is reached.

The fatigue life predictions for beams C80-0, C75-0, C70-0, and C80-20-0 are shown in Figs. 13 and 14 in addition to predictions using Helgason et al. [24]. The predictions using Helgason et al.'s model tends to be more conservative compared to the predictions using the proposed approach. The numbers of cycles predicted in both cases are given in Table 2. From the models proposed by Helgason et al. [24], an endurance limit is assumed below which failure will not occur. This simply means beam C80-20 will not fail under fatigue loading; hence leading to an unsafe fatigue life prediction.

One of the motive of the proposed approach was to develop a conservative means for fatigue life prediction. However, as fatigue load range begins to reduce as in the cases of C70-0 and C80-20 in Fig. 14, the range for acceptable predictions is expected to be wider since variations in the number of cycles to failure corresponding to small or insignificant changes in loading are significantly large due to low induced stresses (as observed in S-N curves for high and low stresses in the literature). This is attributed to the lower fatigue life prediction shown in Fig. 14. In addition, for low fatigue loads and under-reinforced beams, fatigue damage tends to concentrate within the mid-span region; hence the effect of the irreversible strain in the compressive strut on the longitudinal reinforcing bars reduces. Conservatively, the influence of irreversible strains were fully considered in the predictions for the fatigue life of beams C70-0 and C80-20; hence the lower fatigue life predictions.

The strain ( $\epsilon_x$ ) in the longitudinal reinforcing bars per interval of cycles up to failure were also plotted and shown in Fig. 8. As observed, the three phases of fatigue damage evolution are well-defined within the fatigue life for beam C80-0.

The first phase entails a nonlinear deformation. The second phase is characterized by a constant rate of deformation, and the last stage is characterized by an increasing rate of damage leading to failure. The induced force in the steel reinforcement is estimated using Eq. (4), while the residual capacity of the reinforcement is obtained from the product of the residual area and the yield strength. Failure is imminent as both evolutions converge (Figs. 13 and 14).

The predicted results using the proposed approach are conservative and reasonably close to the experimental values; hence, can be implemented in the prediction of fatigue life of deep beams.

The simple strut-tie model considered in this investigation was used based on the low value of the shear-span to effective-depth ratio and the actual load path of force transfer from load point to the support of the tested specimens (see Fig. 10). For larger spans which involves more struts and ties, the same concept of constitutive, compatibility, and equilibrium equations modifications can be employed. In these cases, failure is imminent at a region with the highest stress.

The significance of this approach stems from the fact that the fatigue failure of beams with large shear-span to effective depth ratios (governed by truss action) can also be predicted. In essence, the approach accounts for the progressive crack of reinforcement (shear or longitudinal) and concrete damage; hence, it represents an advantage over previous models which consider fracture of shear reinforcement as the only fatigue limit state.

Although point load was considered in this investigation, in the case of distributed loading, fanning concept of struts is used [22,23]. In the same manner as described for the point load, the governing equations for equilibrium, compatibility, and stress-strain relation can be modified using the referred damage evolution models; however, experimental verifications on these are required.

Small scale beams have been considered in this investigation. Size effect on plain concrete under monotonic and fatigue loading is well-known. The crack growth rate per fatigue loading cycle of plain concrete is higher for larger sizes [41,42]. It is considered expedient that more tests are conducted on lightly-reinforced and sufficiently reinforced large scale beams, while the proposed approach is further scrutinized to ascertain its validity.

## 5. Conclusion

The behaviour of deep beams under fatigue loading has been investigated by conducting tests on small-scale deep beams. The progressive deformations within the shear spans and mid-spans were measured. In all, the rate of deformation was observed to increase as the stress level or stress range increased. It was observed that beams with increased longitudinal reinforcement ratios exhibited higher fatigue life; hence supporting well-known fatigue behaviour of reinforced concrete structures.

The fatigue behaviour was governed by the load transfer mechanism and the induced stresses within the load path. Specimens tested failed by fracture of the longitudinal reinforcement either within the shear span or mid-span region. The results obtained using the modified strut and tie analysis approach gave appropriate fatigue life prediction; hence, providing a reliable means for fatigue analysis of deep beams.

Within the range of failure, the predicted results obtained for the specimens using the proposed approach were found to be conservative. An additional advantage of the proposed fatigue analysis approach stems from the fact that the progressive deformation and the actual mechanism of failure (crushing of concrete or fracture of steel) depending on the governing criterion can be observed.

## Acknowledgments

The authors gratefully acknowledge the Natural Science and Engineering Research Council (NSERC) of Canada and Hatch Ltd for the invaluable contributions and financial support to this research. The authors also acknowledge the assistance received from the Niger Delta Development Commission and the Delta State Government of Nigeria for the duration of this research.

## References

- [1] Okamura H, Farghaly SA, Ueda T. Behaviour of reinforced concrete beams with stirrups failing in shear under fatigue loading. *Proc JSCE* 1981;308:109–23.
- [2] Okamura H, Ueda T. Fatigue behaviour of reinforced concrete beams under shear force. *IABSE Rep* 1982;37:416–22.
- [3] Ueda T. Behaviour in shear of reinforced concrete deep beams under fatigue loading. Dissertation for the degree of Doctor of Engineering, University of Tokyo; 1982.
- [4] Hawkins NM. Fatigue characteristics in bond and shear of reinforced concrete beams. Abeles Symposium. *ACI Pub SP41-10*; 1974. p. 203–36.
- [5] Teng S, Ma W, Tan KH, Kong FK. Fatigue tests of reinforced concrete deep beams. *Struct Eng* 1998;76:347–52.
- [6] Teng S, Ma W, Wang F. Shear strength of concrete deep beams under fatigue loading. *ACI Struct J* 2000;97:572–80.
- [7] Chang TS, Kesler CE. Static and fatigue behaviour in shear of beams with tensile reinforcement. *ACI J* 1958;54:1033–58.
- [8] Stelson TE, Cernica JN. Fatigue properties of concrete beams. *ACI J* 1958;55:255–9.
- [9] Higai T. Fundamental study on shear failure of reinforced concrete beams. *JSCE* 1983;1:25–39.
- [10] Ruhnau J. Influence of repeated loading on the stirrup stress of reinforced concrete beams. *ACI Pub SP42-1*; 1974. p. 169–81.
- [11] Bentz E, Vecchio FJ, Collins MP. Simplified modified compression field theory for calculating shear strength of reinforced concrete elements. *ACI Struct J* 2006;103(4):614–24.
- [12] Mau ST, Hsu TTC. Shear strength prediction for deep beams with web reinforcement. *ACI Struct J* 1987;84:513–23.
- [13] Goransson F, Nordenmark A. Fatigue assessment of concrete foundations for wind power plants. Department of Civil and Environmental Engineering (Master's thesis), Chalmers University of Technology, Goteborg, Sweden; 2011.

- [14] Zanuy C, Fuente P, Albajar L. Effect of fatigue degradation of the compression zone of concrete in reinforced concrete sections. *Eng Struct* 2007;29:2908–20.
- [15] Tamulenas V, Gelazius V, Ramanauskas R. Calculation technique for stress-strain analysis of RC elements subjected to high-cycle compression, vol. 6(5). Moksias: Lietuvos Ateitis; 2014. p. 468–73.
- [16] Cement Association of Canada. *Concrete design handbook*. 3rd ed. Ottawa (Ontario): CAC; 2006.
- [17] EC2. Eurocode 2: design of concrete structures-Part 1-1: General rules for buildings. London, UK: British Standards Institution, BS EN 1992-1-1; 2004.
- [18] ACI 318-14 to ACI 346-09. Manual of concrete practice: Part 3 of 7. American Concrete Institute.
- [19] Torrenti JM, Pijaudier-Cabot G, Reynouard J. Mechanical behaviour of concrete: cyclic and dynamic loading, fatigue of structural concrete. ISTE and Wiley; 2010. p. 185–223.
- [20] Zhang B et al. Effects of loading frequency and stress reversal on fatigue life of plain concrete. *Mag Concr Res* 1996;48:361–75.
- [21] Veeman R, Van Breugel K, koenders E. Effects of corrosion on the fatigue service-life on steel and reinforced concrete beams. In: Concrete-innovation and design, FIB symposium. Copenhagen; 2015.
- [22] Muttoni A, Schwartz J, Thurlimann B. *Design of concrete structures with stress fields*. Birkhauser Basel Boston Berlin 1996.
- [23] Collins MP, Mitchell D. *Prestressed concrete structures*. Canada: Response Publication; 1997.
- [24] Helgason T, Hanson JM, Somes NF, Corley WG, Hognestad E. Fatigue strength of high-yield reinforcing bars. *Natl Cooper Highway Res Program Rep* 1976;161:1–90.
- [25] AASHTO. AASHTO LRFD bridge design specifications, 2008 and 2009 Interim, American Association of State Highway and transportation Officials, Washington DC, 4th ed.; 2007.
- [26] Isojeh MB, Vecchio FJ. Parametric damage of concrete under high-cycle fatigue loading in compression. In: Proc, 9th international conference on fracture mechanics of concrete and concrete structures. FraMCoS-9 2016; 10.21012/FC9.009.
- [27] Isojeh B, El-Zeghayar M, Vecchio FJ. Concrete damage under fatigue loading in uniaxial compression. *ACI Mater J* 114(2): 225–35.
- [28] Isojeh B, El-Zeghayar M, Vecchio FJ. Simplified constitutive model for fatigue behaviour of concrete in compression. *ASCE J Mater*; 2017. doi:[http://dx.doi.org/10.1061/\(ASCE\)MT.1943-5533.0001863](http://dx.doi.org/10.1061/(ASCE)MT.1943-5533.0001863).
- [29] Hognestad E. Confirmation of inelastic stress distribution in concrete. *Proc ASCE* 1954;83(2):1–17.
- [30] Socie D, Dowling NE, Kurath P. Fatigue life estimation of notched members. In: Fracture mechanics: fifteenth symposium. ASTM STP 833; 1984. p. 284–99.
- [31] Jhamb IC, MacGregor JG. Stress concentration caused by reinforcing bar deformations. *ACI SP J* 1974;41:169–82.
- [32] Smith KN, Watson P, Topper TH. A stress-strain function for the fatigue of metals. *J Mater* 1970;5:767–78.
- [33] Dowling NE, Thangjitham NE. An overview and discussion of basic methodology for fatigue. *Fatigue Fract Mech: ASTM STP* 2000;1389(31):3–36.
- [34] Lee Y, Pan J, Hathaway R, Barkey M. *Fatigue testing and analysis: theory and practice*. Elsevier Butterworth-Heinemann; 2005.
- [35] Boller C, Seeger T. *Materials data for cyclic loading*, vol. 5. Amsterdam: Elsevier Science Pubs; 1987.
- [36] Paris P, Gomez MP, Anderson WE. A rational analytical theory of fatigue. *Trend Eng* 1961;13:9–14.
- [37] Rocha M, Bruhwiler E. Prediction of fatigue life of reinforced concrete bridges. In: Biondini, Frangopol, editors. Bridge maintenance, safety, management, resilience and sustainability; 2012. p. 3755–60.
- [38] Herwig A, et al. Reinforced concrete bridges under increased railway traffic loads- fatigue behaviour and safety measures. PhD Thesis No. 4010, Ecole Polytechnique Federale de Lausanne; 2008.
- [39] Farahmand B, Nikbin K. Predicting fracture and fatigue crack growth properties using tensile properties. *Eng Fract Mech* 2008;75:2144–55.
- [40] British Standard. Guide to methods for assessing the acceptability of flaws in metallic structures. BS 7510; 2005.
- [41] Bazant Z, Xu K. Size effects in fatigue fracture of concrete. *ACI Mater J* 1991;88(4):390–9.
- [42] Sain T, Chandra Kishen J. Prediction of fatigue strength in plain and reinforced concrete beams. *ACI Mater J* 2007;104(5):621–8.